

Importance of Hydrodynamic Interactions between Colloids near the Glass Transition¹

Michio TOKUYAMA²

Summary

The paper deals with theoretical, numerical and experimental investigations of hydrodynamic interactions between colloids near the glass transition from a unified point of view based on a mean-field theory proposed recently by the present author. We compare the theory and the two types of computer simulations on hard-sphere systems, a Brownian-dynamics simulation on suspensions of hard spheres, where the hydrodynamic interactions between particles are neglected, and a molecular-dynamics simulation on hard-sphere fluids, with the experiment. Then, we show that the long-time self-diffusion coefficients in those systems can be well described by the same singular function of the volume fraction as that derived in the suspension theoretically by fully taking into account the many-body hydrodynamic interactions, except that the singular point is now replaced by new ones. Thus, we explore how important role the hydrodynamic interactions play near the colloidal glass transition.

1. Introduction

In 1994, we have derived the analytic form for the long-time self-diffusion coefficient by studying the hydrodynamic interactions between particles near the colloidal glass transition [1]. We have shown that there are two types of hydrodynamic interactions. The first is a short-time hydrodynamic interaction, which consists of a short-range hydrodynamic interaction between particles separated by a distance of order a and a long-range hydrodynamic interaction between particles separated by a distance of order ℓ_H , where a is an average particle radius and $\ell_H (= a(9\phi/2)^{-1/2})$ a screening length, ϕ being a particle volume fraction. This becomes important on the time scale of the Brownian relaxation time and leads to a short-time self-diffusion coefficient $D_S^S(\phi)$. This also affects the direct interactions and reduces them. The second is a long-time hydrodynamic interaction, which consists of a long-range hydrodynamic interaction only. This becomes important on the time scale of the structural relaxation time, during which the particle diffuses over

a distance of a particle radius, and leads to a long-time self-diffusion coefficient $D_S^L(\phi)$. The long-time self-diffusion coefficient $D_S^L(\phi)$ is then given by [1, 2]

$$D_S^L(\phi) = D_S^S(\phi) \frac{1 - \frac{9}{32}\phi}{1 + \left(\frac{D_S^S}{D_0}\right) \left(\frac{\phi}{\phi_c^{TO}}\right) \left(1 - \frac{\phi}{\phi_c^{TO}}\right)^{-2}}, \quad (1)$$

where $\phi_c^{TO} = (4/3)^3 / (7 \ln 3 - 8 \ln 2 + 2) \simeq 0.57184\dots$. Here the singular term in the denominator results from the many-body correlations due to the long-range hydrodynamic interactions between particles and hence the singular point ϕ_c^{TO} is determined by the many-body long-range hydrodynamic interactions between particles only. The term $(9/32)\phi$ in the nominator results from the coupled correlations between the short-range hydrodynamic interactions and the direct interactions, where it reduces to 2ϕ if the hydrodynamic interactions are neglected. As is discussed in Sec. 4, this coefficient can describe the experimental data well for volume fractions lower than $\phi \simeq 0.5$, while it deviates from those data for higher volume fractions. Hence the singular point of the experiment is expected to be different from ϕ_c^{TO} .

As of today, there is no first-principle derivation

1. Manuscript received on March 31, 2007.

2. Professor, Institute of Fluid Science, Tohoku University.

of the long-time self-diffusion coefficient which can describe the experimental data for a whole range of volume fractions. The reasons are mainly as follows. The first is because one has to deal with a concentrated system. The second is because the long-range hydrodynamic interactions are described by the Oseen tensor. In this paper, therefore, we compare the experimental data by van Meegen et al [3] with our theoretical and simulation results [1, 4, 5] from a unified point of view based on the mean-field theory [6] and discuss how important role the hydrodynamic interactions between particles play near the colloidal glass transition.

2. Langevin Equations for Suspensions of Polydisperse Hard Spheres

In this section we briefly summarize and discuss the basic equations and concepts for a suspension of hard spheres.

We consider a three-dimensional suspension of N hard spheres with radius a_i and mass m_i ($i = 1, 2, \dots, N$), where the spheres are suspended in an equilibrium fluid with a viscosity η_0 . Here the total volume of the system is V and the temperature is T . We assume that the mass density ρ_0 of each particle is the same as that of fluid. Hence we have $m_i = \frac{4\pi}{3}a_i^3\rho_0$. The distribution of radii is assumed to obey a Gaussian distribution function with standard deviation s divided by the average particle radius a . The volume fraction ϕ is then given by $\phi = \frac{4\pi}{3}a^3n_{eq}(1+3s^2)$, where $n_{eq}(= N/V)$ is the particle number density.

The present system has four characteristic lengths and times [1, 2]; (i) the molecular radius r_m and the microscopic time t_m , (ii) the average moving distance of a particle $r_B(= a(t_B/t_D)^{1/2})$ and the Brownian relaxation time $t_B(= m/\zeta_0)$, (iii) the screening length $\ell_H(= (6\pi a n_{eq})^{-1/2})$, within which the hydrodynamic interactions between particles become important, and the screening time $t_H(= \rho_0 a^2/\eta_0 \phi)$, in which the hydrodynamic interactions become important, and (iv) the average particle radius a and the structural-relaxation time $t_D(= a^2/D_0)$, which is a time required for a particle to diffuse over a distance a , where $D_0(= k_B T/\zeta_0)$ is a single-particle diffusion coefficient, and $\zeta_0(= 6\pi\eta_0 a)$ the friction coefficient. In this paper we deal with concentrated suspensions in which the following inequalities hold: $r_m \ll r_B \leq \ell_H \leq a$ and $t_m \ll t_B \leq t_H \ll t_D$. Depending on the space-time scales of interest, therefore, there exist two char-

acteristic stages. The first is a kinetic stage [K], where the space-time cutoffs (r_{cut}, t_{cut}), which are the minimum wavelength and time of the dynamic process of interest, are set as $r_m \ll r_{cut} \leq \ell_H$ and $t_m \ll t_{cut} \leq t_H$. The second is a suspension-hydrodynamic stage [SH], where $\ell_H \leq a \ll r_{cut}$ and $t_H \ll t_{cut} \leq t_D$.

We first review the Langevin equation in a kinetic stage [K]. Let $\mathbf{X}_i(t)$ and $\mathbf{u}_i(t)(= d\mathbf{X}_i(t)/dt)$ denote the position vector and the velocity of the i th particle at time t , respectively. Then, on the time scale longer than t_B , the velocity $\mathbf{u}_i(t)$ is described by the Markov Langevin equation discussed elsewhere [1, 2]

$$m_i \frac{d}{dt} \mathbf{u}_i(t) = - \sum_{j=1}^N \zeta(\mathbf{X}_{ij}(t)) \cdot \mathbf{u}_j(t) + \sum_{j(\neq i)} \mathbf{F}(\mathbf{X}_{ij}(t)) + \mathbf{R}(\mathbf{X}_i(t), t), \quad (2)$$

where $\mathbf{F}(\mathbf{X}_{ij}(t))$ is the force between particles i and j , and $\mathbf{X}_{ij} = \mathbf{X}_i - \mathbf{X}_j$. Here the random force $\mathbf{R}(\mathbf{X}_i(t), t)$ obeys a Gaussian, Markov process with zero mean and satisfies

$$\langle \mathbf{R}(\mathbf{X}_i, t) \mathbf{R}(\mathbf{X}_j, t') \rangle = 2k_B T \zeta(\mathbf{X}_{ij}(t)) \delta(t - t'), \quad (3)$$

where the brackets $\langle \dots \rangle$ indicate an equilibrium ensemble average. The friction tensors $\zeta(\mathbf{X}_{ij})$ satisfy

$$\zeta(\mathbf{X}_{ij}) = \zeta_{0i}([\mathbf{1} + \mathbf{g}]^{-1})_{ij}, \quad (4)$$

where the tensors $\mathbf{g}(\mathbf{X}_{ij})$ represent the solvent-mediated hydrodynamic interactions between particles i and j , leading to corrections to the friction coefficient $\zeta_{0i}(= \zeta_0 a_i/a)$, and $\mathbf{g}(\mathbf{X}_{ii}) = 0$. The explicit forms of $\mathbf{g}(\mathbf{x}_{ij})$ are given, to order $(a_i/|\mathbf{x}_{ij}|)^3$, by

$$\mathbf{g}(\mathbf{x}_{ij}) = \mathbf{g}_{ij}^O + \mathbf{g}_{ij}^D + O\left(\left(\frac{a_i}{|\mathbf{x}_{ij}|}\right)^4\right), \quad (5)$$

$$\mathbf{g}_{ij}^O = \frac{3}{4} \frac{a_i}{|\mathbf{x}_{ij}|} \left(\mathbf{1} + \frac{\mathbf{x}_{ij}}{|\mathbf{x}_{ij}|} \frac{\mathbf{x}_{ij}}{|\mathbf{x}_{ij}|} \right), \quad (6)$$

$$\mathbf{g}_{ij}^D = \frac{1}{4} \frac{a_i(a_i^2 + a_j^2)}{|\mathbf{x}_{ij}|^3} \left(\mathbf{1} - 3 \frac{\mathbf{x}_{ij}}{|\mathbf{x}_{ij}|} \frac{\mathbf{x}_{ij}}{|\mathbf{x}_{ij}|} \right). \quad (7)$$

The first term \mathbf{g}_{ij}^O of Eq. (5) represents the Oseen tensor and the second term \mathbf{g}_{ij}^D the dipole tensor. Here the hydrodynamic interactions $\mathbf{g}(\mathbf{x}_{ij})$ between particles can be classified into two types, depending on the range of interactions; the long-range hydrodynamic interactions between particles, which lead to divergent integrals, and the short-range hydrodynamic interactions between particles. The force $\mathbf{F}(\mathbf{x}_{ij})$ in Eq. (2)

represents the direct (collision) interactions between particles. Equation (2) is the basic equation to discuss the colloidal suspension of concentrated hard spheres in stage [K]. Because of the long-range interactions appeared in $\mathbf{g}(\mathbf{x}_{ij})$, however, it is beyond our capacity to deal with Eq. (2) analytically. Hence we have suggested two different approaches to discuss the dynamics of suspensions for higher volume fractions in stage [H]. One is to derive a nonlinear diffusion equation for the density fluctuations from Eq. (2). This has been done in Refs. [2, 7] and led to the mean-field theory [6] discussed in the next section. The other is to perform a Brownian-dynamics simulation, starting from Eq. (2). Because of a long-range nature, however, this is not possible right now. In order to investigate the dynamics near the glass transition and compare the simulation results with experiment by van Meegen et al [3], therefore, we have recently performed the simulations for the following two simple cases: (1) Brownian-dynamics (BD) simulations on suspensions without hydrodynamic interactions between particles and (2) molecular-dynamics (MD) simulations on hard-sphere fluids. Those are discussed in Sec. 4.

3. Mean-Field Theory

In this section we briefly summarize the mean-field theory of glass transitions recently proposed [6, 8]. It consists of the following two essential points: (1) a nonlinear mean-field equation for the mean-square displacement and (2) a non-singular long-time self-diffusion coefficient. We next discuss those separately.

3.1 Mean-Field Equations

We consider two types of systems separately, (S) a suspension of colloids where the particles are immersed in the solvent and undergo a Brownian motion, and (M) a hard-sphere fluid where the particles obey a Newton equation. Let $M_2(t)$ the particle mean-square displacement given by

$$M_2(t) = \frac{1}{N} \sum_{i=1}^N \langle [\mathbf{X}_i(t) - \mathbf{X}_i(0)]^2 \rangle, \quad (8)$$

where the brackets denote the equilibrium ensemble average. Then, $M_2(t)$ obeys the following nonlinear equation already described elsewhere [6, 8]:

$$\frac{d}{dt} M_2(t) = 2dD_S^L(\phi) + 2d[s(t) - D_S^L(\phi)]e^{-M_2(t)/\ell^2}, \quad (9)$$

where ϕ denotes a volume fraction, and $D_S^L(\phi)$ a long-time self-diffusion coefficient. Eq. (9) describes not only the dynamics of the suspension but also that of the molecular system. The difference between two systems appears only in the short-time behavior, which is described by the function $s(t)$ given by

$$s(t) = \begin{cases} D_S^S(\phi) & \text{for (S),} \\ \frac{v_0^2}{d}t & \text{for (M),} \end{cases} \quad (10)$$

where $v_0(= (dk_B T/m)^{1/2})$ denotes the average velocity of a particle and m the average particle mass. The short-time self-diffusion coefficient $D_S^S(\phi)$ results from the short-range hydrodynamic interactions between particles and is given by Eq. (11) of Ref. [1]. Here the mean-free path $\ell(\phi)$ is a free length in which a particle can move freely without any interactions between particles. This is determined by fitting the solution of Eq. (9) with data.

Eq. (9) is easily solved to give a formal solution

$$M_2(t) = 2dD_S^L t + \ell^2 \ln \left[e^{-2dt/\tau_\beta} + \kappa \left\{ 1 - \left(1 + c \frac{2dt}{\tau_\beta} \right) e^{-2dt/\tau_\beta} \right\} \right] \quad (11)$$

with

$$\kappa = \begin{cases} \frac{\tau_\beta}{\tau_f} & \text{for (S),} \\ \frac{1}{2d^2} \left(\frac{\tau_\beta}{\tau_f} \right)^2 & \text{for (M),} \end{cases} \quad (12)$$

where $c = 0$ for (S) and $c = 1$ for (M). Here $\tau_\beta(= \ell^2/D_S^L)$ represents a β -relaxation time, which is a time for a particle to diffuse over a distance of order ℓ with the diffusion coefficient D_S^L and τ_f a mean-free time given by

$$\tau_f = \begin{cases} \ell^2/D_S^S & \text{for (S),} \\ \ell/v_0 & \text{for (M).} \end{cases} \quad (13)$$

Within τ_f each particle can move freely without any interactions between particles. In addition to two time scales, τ_β and τ_f , there exists another time scale τ_γ for higher volume fractions [6, 8]. The time τ_γ denotes the caging time at which the particle is trapped in a cage which is mostly formed by neighboring particles. On the other hand, the time τ_β denotes the escape time at which the particles can escape their cages.

In order to analyze the data by using Eq. (11), the length \mathbf{X}_i and the time t are scaled by a and t_0 as

$$\hat{\mathbf{X}}_i = \mathbf{X}_i/a, \quad \hat{t} = t/t_0, \quad (14)$$

respectively. Here the fundamental time t_0 is given by

$$t_0 = \begin{cases} a^2/D_0 & \text{for (S),} \\ a/v_0 & \text{for (M),} \end{cases} \quad (15)$$

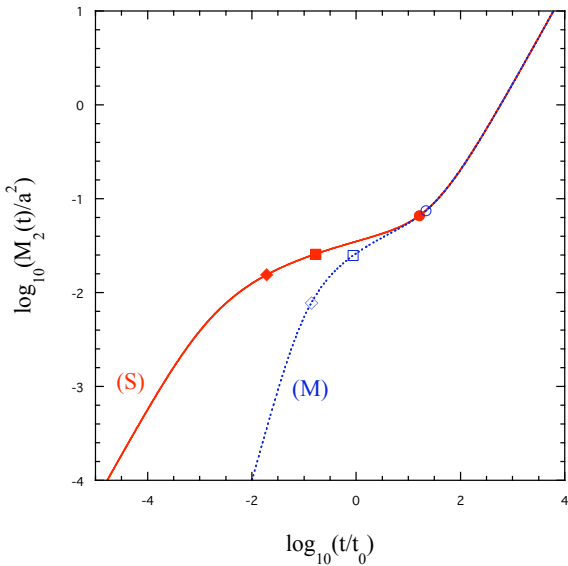


Fig.1 A log-log plot of the mean-square displacement $M_2(t)$ versus time at $\log_{10}(D_S^L/\Delta_0) = -3.565$ and $\ell = 0.1386$, where $d = 3$. The solid line stands for (S) and the dotted line for (M). The filled symbols indicate the times τ_β (\circ), τ_γ (\square), and τ_f (\diamond) for (S), while the open symbols for (M).

where D_0 is a single-particle diffusion constant. Then, the diffusion coefficient D_S^L is scaled as D_S^L/Δ_0 , where

$$\Delta_0 = \begin{cases} D_0 & \text{for (S),} \\ av_0 & \text{for (M),} \end{cases} \quad (16)$$

In Fig. 1, a typical example of the formal solution given by Eq. (11) is shown for two types of systems (S) and (M) at $D_S^L/\Delta_0 = 10^{-3.565}$ and $\ell/a = 0.1386$.

3.2 Long-Time Self-Diffusion Coefficients

The second important feature of MFT is a prediction of the non-singular long-time self-diffusion coefficient. In 1994 Tokuyama and Oppenheim [1, 2] have studied the hydrodynamic interactions between particles in the concentrated hard-sphere suspensions and derived the long-time self-diffusion coefficient $D_S^L(\phi)$ given by

$$D_S^L(\phi) = D_S^S(\phi) \frac{1 - \frac{9}{32}\phi}{1 + \left(\frac{D_S^S}{D_0}\right) \left(\frac{\phi}{\phi_c^{TO}}\right) \left(1 - \frac{\phi}{\phi_c^{TO}}\right)^{-2}}, \quad (17)$$

where $\phi_c^{TO} = (4/3)^3/(7\ln 3 - 8\ln 2 + 2) \simeq 0.57184\dots$. The short-time self-diffusion coefficient $D_S^S(\phi)$ results from the many-body short-time hydrodynamic interactions between particles and is given by Eq. (11) of

Ref. [1]. Here the singular term in the denominator results from the many-body correlations due to the long-range hydrodynamic interactions between particles and hence the singular point ϕ_c^{TO} is determined by the many-body long-range hydrodynamic interactions between particles only. The term $(9/32)\phi$ in the nominator results from the coupled correlations between the short-range hydrodynamic interactions and the direct interactions, where it reduces to 2ϕ if the hydrodynamic interactions are neglected. Recently, this coefficient was extended to discuss the other systems as [6]

$$\frac{D_S^L(p)}{\Delta_0} = \frac{D_S^S(p)}{D_0} \frac{1 - Cp}{1 + \epsilon \left(\frac{D_S^S}{D_0}\right) \left(\frac{p}{p_c}\right) \left(1 - \frac{p}{p_c}\right)^{-2}}, \quad (18)$$

where p is a control parameter, and p_c , ϵ , and C are unknown coefficients to be determined by fitting with data. Here the singular term in the denominator is considered to result from the long-time correlations due to the many-body interactions between particles and the term Cp from the coupling effect between hydrodynamic interactions and different interactions. In Ref. [6], Eq. (18) was shown to describe the data of the long-time self-diffusion coefficient in diversely different systems partially well. Since all the data deviate from Eq. (18) above p_c , however, the non-singular type of the long-time self-diffusion coefficient was also proposed in [7, 9] by introducing a transformation from p to a new parameter p_n by

$$p_n = p + 10^{-\alpha} \frac{p}{p_c(p_c - p)}, \quad (19)$$

where α is a positive constant to be determined by fitting. One may first solve Eq. (19) for p and then insert it into Eq. (18). Then, the coefficient $D_S^L(p_n)$ shows a non-singular function of p_n . As discussed in Ref. [9], the coefficients ϵ and α do not depend on the details of interactions if the main interactions are the same in different systems, while p_c and C strongly depend on the details. As is shown later, we have $\epsilon = 1$ and $\alpha = 4.86$ for the colloidal suspensions and the hard-sphere fluids with arbitrary size polydispersity.

4. Analyses by MFT

The diffusion coefficient D_S^L and the mean-free path ℓ are determined by fitting the solution given by Eq. (11) with the experimental data and the simulation results. In the following, we analyze the experimental data for colloidal suspensions of hard spheres

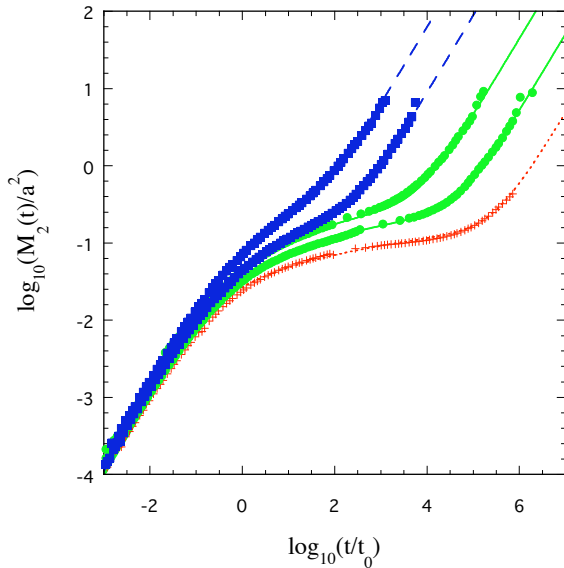


Fig.2 A log-log plot of the mean-square displacement $M_2(t)$ versus time for different volume fractions; $\phi=0.502, 0.538, 0.558, 0.566,$ and 0.583 (from left to right). The symbols indicate the experimental results from Ref. [3] in a liquid state (\square), a supercooled state (\circ), and a glass state ($+$). The mean-field results given by Eq. (11) are given by the dashed lines in a liquid state, the solid lines in a supercooled state, and the dotted line in a glass state.

and the simulation results for hard-sphere systems separately and discuss their mean-square displacements and long-time self-diffusion coefficients only. Here the mean-free path ℓ was already discussed elsewhere [6, 8].

4.1 Analyses of Experimental Data

We first analyze the experimental data obtained by van Megen et al [3, 10] for colloidal suspensions of neutral hard spheres with 6% polydispersity. The main forces acting on hard spheres are a force exerted by the fluctuating fluid on spheres, undergoing a Brownian motion, a hydrodynamic interaction between particles, and a direct interaction between particles. The control parameter is a volume fraction ϕ , where the polydispersity s is set as $s = 0.06$. In order to analyze the data by MFT, we scale space and time by a and $t_0(= a^2/D_0)$, respectively, where $a=200\text{nm}$, $D_0 = 0.31 \times 10^{-12}\text{m}^2/\text{s}$, and $T = 20.4^\circ\text{C}$. By adjusting the length ℓ and the coefficient D_S^L , one can fit Eq. (11) with the experimental data. In Fig. 2 we show the

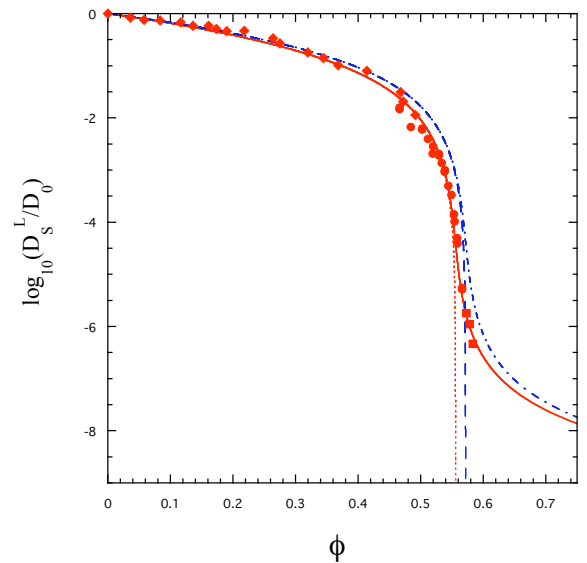


Fig.3 A log plot of $D_S^L(\phi)/D_0$ versus ϕ . The filled circles indicate the experimental results from Ref. [3], the filled diamonds from Ref. [10], and the filled squares the values predicted by MFT. The dashed line indicates the singular function given by Eq. (17), the dashed-dot line its non-singular function obtained by using Eq. (19) in Eq. (17), the dotted line the singular function given by Eq. (18), and the solid line its non-singular function obtained by using Eq. (19) in Eq. (18), where $\epsilon = 1$, $\alpha \simeq 4.86$, $\phi_c \simeq 0.5560$, and $C \simeq 9/32$.

fitting results for $M_2(t)$ at different volume fractions. As discussed in Ref. [6], there exist three states, a liquid state for $\phi < \phi_\beta(\simeq 0.544)$, a supercooled state for $\phi_\beta \leq \phi < \phi_g(\simeq 0.580)$, and a glass state for $\phi_g \leq \phi$, where ϕ_β and ϕ_g denote the supercooled point and the glass transition point, respectively. The mean-field results agree very well with the experimental data.

By fitting, one can obtain the long-time-self-diffusion coefficient D_S^L . In Fig. 3, those fitting results are shown. By using Eq. (18), one can first find the singular function with $\epsilon = 1$, $\phi_c \simeq 0.556$, and $C \simeq 9/32$. By using Eq. (19), one can then find the non-singular function with $\alpha \simeq 4.86$. Both singular and non-singular functions are compared with the experimental results in Fig. 3 together with the theoretical diffusion coefficient given by Eq. (17). Here we should note that the old experimental results of Ref. [10] are well described by the theoretical result given by Eq. (17) in which ϕ_c is determined only by the

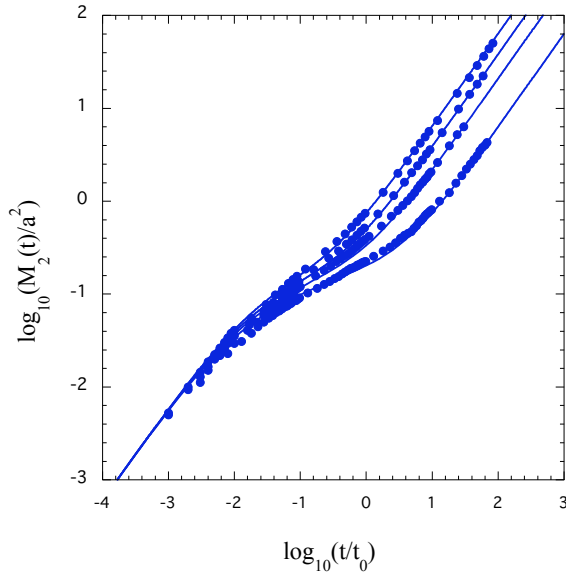


Fig.4 A log-log plot of the mean-square displacement $M_2(t)$ versus time for different volume fractions; $\phi=0.5000, 0.5200, 0.5400,$ and 0.5600 (from left to right). The symbols indicate the simulation results from Ref. [4] in a liquid state. The solid lines indicate the mean-field results given by Eq. (11).

many-body hydrodynamic interactions, while the recent experimental results of Ref. [3] are well described by the extended coefficient given by Eq. (18) with $\epsilon = 1$, $\alpha \simeq 4.86$, $\phi_c \simeq 0.5560$, and $C \simeq 9/32$. Thus, it turns out that the singular point $\phi_c^{TO} \simeq 0.57184\dots$ is further reduced to the smaller value 0.5560 by the many-body direct interactions. We also mention that the singular point ϕ_c must be corrected as $\phi_c = 0.5560$ which is different from the value 0.5640 discussed earlier in Ref. [6]. This is reasonable because one can fit Eq. (18) with all data if one takes $\phi_c = 0.5560$, while one can fit it only with the recent experimental data for $\phi > 0.4500$ by taking $\phi_c = 0.5640$.

4.2 Analyses of BD Simulation results

We next analyze the simulation results for the suspension of hard spheres in stage [H] [4]. Because of the long-range nature of the hydrodynamic interactions, it is not possible to perform the computer simulations starting from Eq. (2). As mentioned earlier, we neglect the hydrodynamic interactions. Hence the main forces acting on hard spheres are a force exerted by the fluctuating fluid on spheres, undergoing a Brownian motion, and a direct interaction between

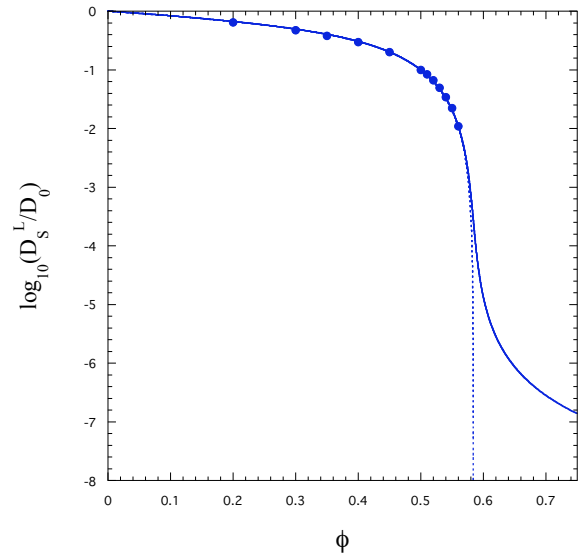


Fig.5 A log plot of the long-time self-diffusion coefficient $D_S^L(\phi)$ versus volume fraction. The filled circles indicate the simulation results from Ref. [4]. The dotted line indicates the singular function given by Eq. (18), and the solid line its non-singular function obtained by using Eq. (19) in Eq. (18) where $\epsilon = 1$, $\alpha \simeq 4.86$, $\phi_c \simeq 0.5843$, and $C = 0$.

particles. Since we are only interested in the dynamics in stage [H], we safely put $m_i(d/dt)\mathbf{u}_i(t) \simeq 0$ on the time scale of order t_D . Then, Eq. (2) reduces to the stochastic diffusion equation

$$\frac{d}{dt}\mathbf{X}_i(t) = \frac{1}{\zeta_{0i}} \sum_{j(\neq i)} \mathbf{F}(\mathbf{X}_{ij}(t)) + \mathbf{f}_i(t) \quad (20)$$

with the random velocity $\mathbf{f}_i(t)$, which satisfies

$$\langle \mathbf{f}_i(t) \rangle = \mathbf{0}, \quad (21)$$

$$\langle \mathbf{f}_i(t)\mathbf{f}_j(t') \rangle = 2D_{0i}\delta_{ij}\delta(t-t')\mathbf{1}, \quad (22)$$

where $D_{0i}(=k_B T/\zeta_{0i})$ denotes the free-diffusion constant of i th particle. Here the forces $\mathbf{F}(\mathbf{X}_{ij})$ describes only the direct interactions between particles. We then employ the forward Euler difference scheme to integrate Eq. (20) with time step $10^{-3}t_D$ under periodic boundary and appropriate initial conditions, where $s = 0.06$ and $N = 10976$. In order to equilibrate the system, we wait for a long time whose time is called a waiting time t_w .

In Fig. 4, a log-log plot of the mean-square displacement $M_2(t)$ is shown versus time for different volume fractions at $t_w \simeq 10^5 t_0$. The simulation results are well described by the mean-field equation (11). In

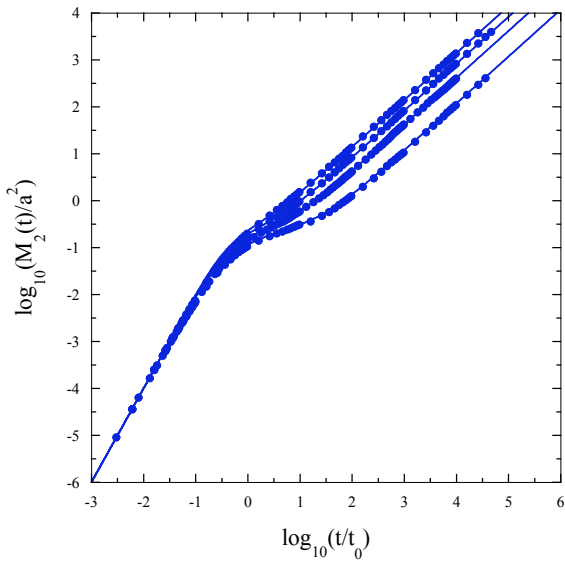


Fig.6 A log-log plot of the mean-square displacement $M_2(t)$ versus time for different volume fractions; $\phi=0.5000, 0.5200, 0.5400,$ and 0.5600 (from left to right). The symbols indicate the simulation results from Ref. [5, 11] and the solid lines the mean-field results.

Fig. 5, a log plot of the long-time self-diffusion coefficient $D_S^{L(S)}(\phi)$ is shown versus volume fraction. The fitting values are well described by both the singular and the non-singular functions given by Eq. (18) as

$$\frac{D_S^{L(S)}(\phi)}{D_0} = \frac{1}{1 + \epsilon \left(\frac{D_S^S}{D_0} \right) \left(\frac{\phi}{\phi_c} \right) \left(1 - \frac{\phi}{\phi_c} \right)^{-2}}, \quad (23)$$

where $\epsilon = 1$, $\alpha \simeq 4.86$, $\phi_c \simeq 0.5843$, and $C = 0$. We note that there is no data available for $\phi \geq \phi_m (\simeq 0.5625)$ since the crystallization occurs at the melting point ϕ_m . We mention here that the coefficient α is the same as those obtained in the experiment and the theory, while the singular point ϕ_c are different from each other. Thus, it does not depend on whether the hydrodynamic interactions exist or not but do depend on the direct interactions. This will be discussed next.

4.3 Analyses of MD Simulation results

In order to check how the direct interactions play an role in the suspensions, we only consider those interactions here in the model system of hard spheres [5, 11], which consists of only N particles in the system of volume V surrounded by the heat bath with temperature T . The particles obey the Newton equations with the forces $\mathbf{F}(\mathbf{X}_{ij})$. Here the forces $\mathbf{F}(\mathbf{X}_{ij})$

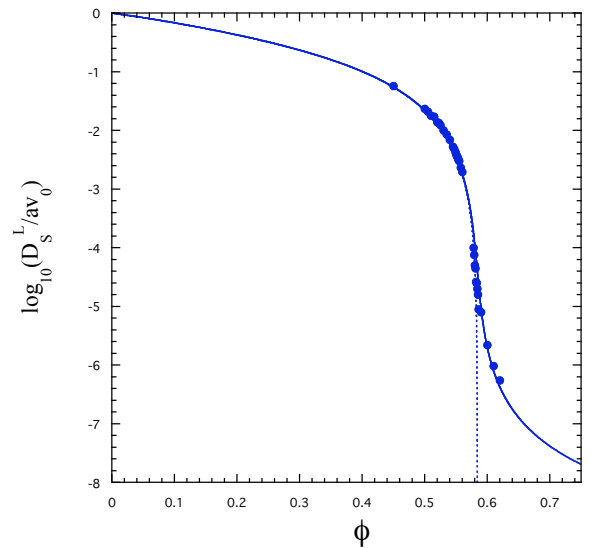


Fig.7 A log plot of the long-time self-diffusion coefficient $D_S^L(\phi)$ versus volume fraction. The filled circles indicate the simulation results from Ref. [5] at the waiting time of order $10^5 t_0$. The dotted line indicates the singular function given by Eq. (18), and the solid line its non-singular function obtained by using Eq. (19) in Eq. (18) where $\epsilon = 1$, $\alpha \simeq 4.86$, $\phi_c \simeq 0.5843$, and $C = 0$.

describe only the direct interactions between particles. Those equations are solved under periodic boundary and appropriate initial conditions, together with the momentum and the energy conservation laws, at $N = 10976$ and $s = 0.06$, where space and time are scaled by a and t_0 , respectively.

In Fig. 6, a log-log plot of $M_2(t)$ is shown versus time for different volume fractions at $t_w \simeq 2 \times 10^5 t_0$. At the waiting time of order $10^5 t_0$ the metastable state can still exist even above the melting point $\phi_m (\simeq 0.5625)$, leading to the re-entrant melting [5]. After a long time of order $2 \times 10^5 t_0$, however, the system is finally crystallized for $\phi \geq \phi_m$. Hence in Fig. 6 we only plot the results for $\phi < \phi_m$. Here the melting point ϕ_m is the same as that obtained in the suspension without the hydrodynamic interactions. This means that without the hydrodynamic interactions between particles the melting point is determined by only the direct interactions and the Brownian motion does not play any role in determining the value of ϕ_m .

In Fig. 7, a log plot of $D_S^{L(M)}(\phi)$ is shown versus volume fraction at $t_w \simeq 10^5 t_0$. The simulation results are well described by both the singular and the non-

singular functions given by Eq. (18) as

$$\frac{D_S^{L(M)}(\phi)}{av_0} = \frac{D_S^S(\phi)}{D_0} \frac{1}{1 + \epsilon \left(\frac{D_S^S}{D_0}\right) \left(\frac{\phi}{\phi_c}\right) \left(1 - \frac{\phi}{\phi_c}\right)^{-2}}, \quad (24)$$

where $\epsilon = 1$, $\alpha \simeq 4.86$, $\phi_c \simeq 0.5843$, and $C = 0$. The results in the metastable state obeys the non-singular function at $t_w \simeq 10^5 t_0$, although those disappear at $t_w \geq 2 \times 10^5 t_0$ because of crystallization. All the coefficients are the same as those in the suspension without the hydrodynamic interactions. This means that both systems are identical from each other. The difference appears only in the following two points. One is the short-time behavior; a free diffusion process described by $M_2(t) \simeq 6D_0 t$ for (S) and a ballistic motion given by $M_2(t) \simeq (v_0 t)^2$ for (M). The second is the short-time self-diffusion coefficients in both systems. In fact, we have the following relation between two coefficients $D_S^{L(S)}$ and $D_S^{L(M)}$: [4]

$$\frac{D_S^{L(M)}(\phi)}{av_0} = \frac{D_S^S(\phi)}{D_0} \frac{D_S^{L(S)}(\phi)}{D_0}. \quad (25)$$

Hence the long-time self-diffusion coefficient in (S) becomes identical to that in (M) if one takes into account the short-time hydrodynamic interactions between particles from the beginning in (S) since $D_S^S(\phi)$ results from the short-range many-body hydrodynamic interactions between particles [1]. Thus, an important role of the short-range hydrodynamic interactions between particles is explored. However, both simulation results with 6% polydispersity do not agree with the experimental results. We next discuss this.

5. Role of Hydrodynamic Interactions near the Colloids Glass Transition

We now discuss the important role of the hydrodynamic interactions between particles near the colloidal glass transition. In Fig. 8, all the long-time self-diffusion coefficients discussed in the previous sections are plotted versus volume fraction together with the theoretical results and the mean-field results. We have four different long-time self-diffusion coefficients. The first one is the experimental coefficient $D_S^{L(E)}$, which is well described by

$$\frac{D_S^{L(E)}(\phi)}{D_0} = \frac{D_S^S(\phi)}{D_0} \frac{1 - (9/32)\phi}{1 + \left(\frac{D_S^S}{D_0}\right) \left(\frac{\phi}{\phi_c^E}\right) \left(1 - \frac{\phi}{\phi_c^E}\right)^{-2}}, \quad (26)$$

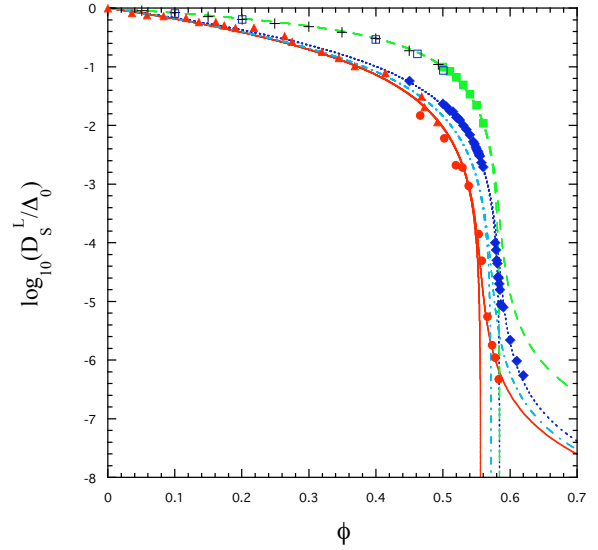


Fig.8 A log plot of the long-time self-diffusion coefficient $D_S^L(\phi)$ versus volume fraction. The filled circles indicate the experimental results from Ref. [3], the filled triangles the experimental results from Ref. [10], the filled diamonds the simulation results from Ref. [5] at $t_w \simeq 10^5 t_0$, the filled squares the simulation results from Ref. [4] at $t_w \simeq 10^5 t_0$, the open squares the simulation results from Ref. [12], and the pluses the simulation results from Ref. [13]. The solid line indicates the singular and the non-singular functions given by Eq. (18) with $\epsilon = 1$, $\alpha \simeq 4.86$, $\phi_c \simeq 0.5560$, and $C = 9/32$, the dashed line those given by Eq. (23) with $\epsilon = 1$, $\alpha \simeq 4.86$, $\phi_c \simeq 0.5843$, and $C = 0$, and the dotted line those given by Eq. (24) with $\epsilon = 1$, $\alpha \simeq 4.86$, $\phi_c \simeq 0.5843$, and $C = 0$. The dot-dashed line is the theoretical functions given by Eq. (17) with $\epsilon = 1$, $\alpha \simeq 4.86$, $\phi_c \simeq 0.57185$, and $C = 9/32$.

where $\phi_c^E \simeq 0.5560$. The main mechanisms here are the direct interactions between particles and the hydrodynamic interactions between particles. The singular point ϕ_c^E results from the many-body correlations due to the direct interactions and the long-range hydrodynamic interactions. The second is the theoretical coefficient $D_S^{L(T)}$, which is well described by

$$\frac{D_S^{L(T)}(\phi)}{D_0} = \frac{D_S^S(\phi)}{D_0} \frac{1 - (9/32)\phi}{1 + \left(\frac{D_S^S}{D_0}\right) \left(\frac{\phi}{\phi_c^{TO}}\right) \left(1 - \frac{\phi}{\phi_c^{TO}}\right)^{-2}}, \quad (27)$$

where $\phi_c^{TO} = (4/3)^3 / (7 \ln 3 - 8 \ln 2 + 2) \simeq 0.57184 \dots$. The main mechanisms here are the direct interactions between particles and the hydrodynamic interactions between particles. The singular point ϕ_c^{TO} results from

the many-body long-range hydrodynamic interactions only. The third is the coefficient $D_S^{L(M)}$ for the hard-sphere systems, which is well described by

$$\frac{D_S^{L(M)}(\phi)}{av_0} = \frac{D_S^S(\phi)}{D_0} \frac{1}{1 + \left(\frac{D_S^S}{D_0}\right) \left(\frac{\phi}{\phi_c^M}\right) \left(1 - \frac{\phi}{\phi_c^M}\right)^{-2}}, \quad (28)$$

where $\phi_c^M \simeq 0.5843$. The main mechanism is the direct interactions between particles. The singular point ϕ_c^M results from the many-body direct interactions only. The last is the coefficient $D_S^{L(S)}$ for the suspension without the hydrodynamic interactions between particles, which is well described by

$$\frac{D_S^{L(S)}(\phi)}{D_0} = \frac{1}{1 + \left(\frac{D_S^S}{D_0}\right) \left(\frac{\phi}{\phi_c^S}\right) \left(1 - \frac{\phi}{\phi_c^S}\right)^{-2}}, \quad (29)$$

where $\phi_c^S \simeq 0.5843$. The main mechanisms here are the direct interactions between particles and the Brownian motion. Since the singular point ϕ_c^S is the same as ϕ_c^M , it also results from the direct interactions only. The Brownian motion does not play any role in the diffusion coefficient. For comparison, the old simulation results from [12, 13] are also plotted in Fig. 8. They are described by Eq. (29) very well. In Table 1, the values of the relevant parameters are listed. In order to obtain Eq. (26) from Eq. (29), therefore, we need three steps. The first is to include the many-body short-range hydrodynamic interactions, leading to D_S^S . Then, one obtains Eq. (28). The second is to include the coupling effects between the short-range hydrodynamic interactions and the direct interactions, leading to $(9/32)\phi$. The direct interactions lead to ϕ_c^M , while the long-range hydrodynamic interactions lead to ϕ_c^{TO} . In order to obtain ϕ_c^E , therefore, the last step is to include the long-range hydrodynamic interactions, which reduces ϕ_c^M to ϕ_c^E . Thus, this suggests that in addition to the direct interactions, both the long-range and the short-range hydrodynamic interactions are indispensable to explain the experimental results.

6. Summary

In the present paper, we have investigated the importance of the hydrodynamic interactions between particles from a unified viewpoint based on the mean-field theory. We have explored the roles of two types of hydrodynamic interactions, the short- and the long-time hydrodynamic interactions, which were theoretic-

Table 1 The parameters α , ϵ , ϕ_c , ϕ_m , and C for different systems at $s = 0.06$. HSS(E) indicates the experimental results for the hard-sphere suspension [3], HSS(T) the theoretical results for the hard-sphere suspension [1], HSS(S) the simulation results for the hard-sphere suspension without hydrodynamic interactions [4, 12, 13], and HSF(S) the simulation results for the hard-sphere fluid [5].

System	α	ϵ	ϕ_c	ϕ_m	C
HSS(E)	4.86	1.0	0.5560	-	9/32
HSS(T)	4.86	1.0	0.5718	-	9/32
HSS(S)	4.86	1.0	0.5843	0.5625	0
HSF(S)	4.86	1.0	0.5843	0.5625	0

cally discussed in Refs. [1, 2]. Thus, we have shown that both types of hydrodynamic interactions are indispensable to explain the experimental results in addition to the direct interactions. Especially, the long-time hydrodynamic interactions have been shown to play an essential role in determining the dynamics of the long-time diffusion process near the colloidal glass transition together with the direct interactions.

Tokuyama and Oppenheim [1, 2] have mainly studied the long-time hydrodynamic interactions, leading to the singular point ϕ_c^{TO} . However, the experimental data have suggested the singular point ϕ_c^E , which is determined not only by the long-time hydrodynamic interactions but also by the direct interactions. In order to check this, a simulation must be encouraged to be performed for Eq. (2). This will be discussed elsewhere.

Acknowledgments

The author is grateful to Y. H. Hwang, I. Oppenheim, Y. Terada, and E. R. Weeks for fruitful discussions. He also thanks W. van Meegen for providing him with his experimental data. This work was partially supported by Grants-in-aid for Science Research with No. 18540363 from Ministry of Education, Culture, Sports, Science and Technology of Japan.

References

- [1] M. Tokuyama and I. Oppenheim: Dynamics of Hard-Sphere Suspensions, *Phys. Rev. E*, Vol.50 (1994), pp.R16–R19.
- [2] M. Tokuyama and I. Oppenheim: On the Theory of Concentrated Hard-Sphere Suspensions, *Phys-*

- ica A, Vol.216 (1995), pp.85–119.
- [3] W. van Meegen, T. C. Mortensen, S. R. Williams and J. Müller: Measurement of the Self-Intermediate Scattering Function of Suspensions of Hard Spherical Particles near the Glass Transition, *Phys. Rev. E*, Vol.58 (1998), pp.6073–6085.
- [4] M. Tokuyama, H. Yamazaki and Y. Terada: Test of Mean-Field Equations for Two Types of Hard-Sphere Systems by a Brownian-Dynamics Simulation and a Molecular-Dynamics Simulation, *Phys. Rev. E*, Vol.67 (2003), pp.0.2403-1–062403-4.
- [5] M. Tokuyama and Y. Terada: How Different is a Hard-Sphere Fluid from a Suspension of Hard-Sphere Colloids near the Glass Transition?, *Physica A*, Vol.375 (2007), pp.18-36.
- [6] M. Tokuyama: Mean-Field Theory of Glass Transitions, *Physica A*, Vol.364 (2006), pp.23–62.
- [7] M. Tokuyama: Slow Dynamics of Equilibrium Density Fluctuations in Suspensions of Colloidal Hard Spheres near the Glass Transition, *Phys. Rev. E*, Vol.62 (2000), pp.R5915–R5918.
- [8] M. Tokuyama: Similarities in Diversely Different Glass-Forming Systems, *Physica A*, Vol.378 (2007), pp157-166.
- [9] M. Tokuyama, T. Narumi and E. Kohira: Mapping from a Complex Glass-Forming System to a Simpler One near their Glass Transitions, *to be submitted to Physica A*, February, 2007.
- [10] W. van Meegen and S. M. Underwood : Tracer diffusion in concentrated colloidal dispersions. III. Mean squared displacements and self-diffusion coefficients, *J. Chem. Phys.*, Vol.91 (1989), pp.552–559.
- [11] M. Tokuyama and Y. Terada: Slow Dynamics and Re-entrant Melting in a Polydisperse Hard-Sphere Fluid, *J. Phys. Chem. B*, Vol.109 (2005), pp.21357–21363.
- [12] I. Moriguchi: Self-Diffusion Coefficient in Dense Hard Sphere Colloids, *J. Chem. Phys.*, Vol.106 (1997), pp.8624–8625.
- [13] J. L. Barrat, W. Götze and A. Latz: The Liquid-Glass Transition of the Hard-Sphere System, *J. Phys. Condens. Matter*, Vol.1 (1989), pp.7163–7170.